Electronic Supplementary Material (ESI) for Physical Chemistry Chemical Physics

Supplemental

The Spectroscopic Ruler Revisited at 77 K

V. Hirschfeld, H. Paulsen, C. G. Hübner

University of Lübeck, Institute of Physics, Ratzeburger Allee 160, 23562 Lübeck

1. Photophysical properties of the dyes

All experiments concerning the photophysical properties were ensemble measurements. They were carried out in 50 mM sodium phosphate buffer, pH 7.0, (Carl Roth, Karlsruhe, Germany) containing 7.5 % (w/v) of trehalose (D(+)-trehalose, Carl Roth).

1.1. Time resolved anisotropy

For time resolved anisotropy measurements both a pulsed laser operating at 470 nm, 20 MHz (Picoquant, Berlin, Germany) and a counting electronic recording time-tagged and time-resolved (TTTR) (Timeharp 200, Picoquant) were implemented in the same set-up (see Section 3.1.). The donor dye Alexa Fluor 488 (AF488) was excited with linear polarized light. The emitted light passed a band pass filter (HQ 532/70, Chroma, Bellows Falls, VT) before it was split into horizontal polarized and vertical polarized light by a polarizing beamsplitter (Melles Griot, Bensheim, Germany). The concentration of the peptides was 200 nM and 1 µM for measurements at room temperature and at 77 K. (Anisotropy measurements were only conducted for the donor due to a missing pulsed laser operating at 594 nm required for the acceptor dye.)

The anisotropy is a measure of the reorientation of the transition dipole after excitation, and thus provides information on how strong the movement of molecules is inhibited. While the orientation of the molecule should be frozen at 77 K, the dipole itself might change in time.

To gain an insight into the re/orientation of the dipoles time resolved anisotropy measurements were carried out at room temperature and at 77 K (FIG. S1).

Due to the usage of an objective with high numerical aperture (CFI Achromat 60 X, NA 0.8, Nikon, Kingston, U.K.) causing polarization scrambling the anisotropy r is defined as $r = (I_P - I_S)/(I_P + K \cdot I_S)$ with K = 1.48, a constant, which takes account of the scrambling[1], and I_P and I_S, the emission intensities parallel and perpendicular polarized to the excitation polarization, respectively.

FIG. S1 shows the time dependent anisotropy decay of AF488 attached to proline 6 at ambient temperature indicating free rotation in solution. The decay, fitted with an exponential, leads to a rotation correlation time of (0.71 ± 0.03) ns. In contrary, at 77 K the peptide chains as well as the fluorophores and their transition moments are fixed, so that the anisotropy remains constant in time.

The resulting steady state anisotropy of 0.34 is close to the value of 0.4 expected for immobile dipoles. The small deviation from the expected theoretical value might be attributed to imperfect correction of the polarization scrambling.

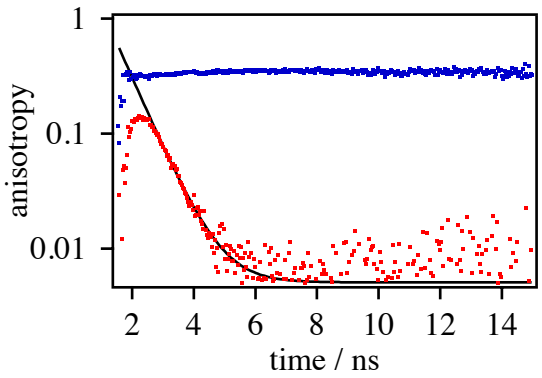

FIG. S1: Anisotropy decay of AF488 bound to proline 6 at room temperature and at 77 K: The anisotropy decays rapidly at ambient temperature (red dots) due to free rotation of the dye. The exponential fit of the decay (black line) reveals a rotation correlation time of (0,71

± 0,03) ns. In the frozen state (blue dots) the anisotropy remains constant indicating fixed molecules.

1.2. Fluorescence lifetime of AF488

The same set-up and concentrations of peptides as for anisotropy measurements (see Suppl. Section 1.1.) were used to measure the lifetime of the donor dye (AF488) at ambient temperature and at 77 K. The fluorescence decay of AF488 bound to proline 6 is shown in FIG. S2. Fitting with an exponential reveals a fluorescence lifetime of (4.1 ± 0.1) ns at ambient temperature and a decreased lifetime of (3.2 ± 0.1) ns in the frozen state. This lifetime is used for an estimation of the quantum yield of the donor in the frozen state required for the determination of the Förster-radius (see Suppl. Chapter 4).

The reduction of the fluorescence lifetime upon freezing is unexpected. Fluorescence lifetimes as well as quantum yields are known to depend on solvents and temperature[2]. Typically, interactions and therewith non-fluorescent processes are minimized in a fixed matrix leading to higher photostability and thus to longer fluorescence lifetimes[3, 4]. The decrease of the fluorescence lifetime, as in our case, can be explained by the nearby interface between ice and glass (see FIG. S2b). It is known that the fluorescence lifetime decreases as a fluorophore gets closer to an interface with a change to a higher refractive index[5]. Here, the dye is embedded in amorphous ice, which itself is enclosed by liquid nitrogen on top and by glass at the bottom. That means, compared with the refractive index of glass (n = 1.52), the dye is in a medium with a lower refractive index (n = 1.31). Thus, the decreased lifetime is assumed to be caused by the interface ice / glass. The change of the refractive index in direction of the liquid nitrogen (n = 1.21) is smaller so that it has a minor influence on the fluorescence lifetime.

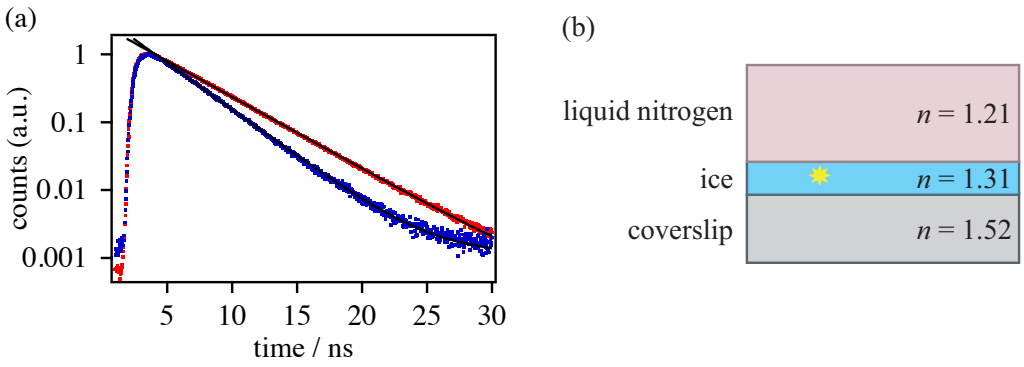

FIG. S2: Fluorescence decay and scheme of the environment of the dye. a) Fluorescence decay of AF488 bound to proline 6 at room temperature (red dots) and at 77 K (blue dots). The corresponding exponential fits are black. The fluorescence lifetime is reduced in the frozen matrix due to the proximity of the interface between amorphous ice and glass. b) Scheme of the different layers surrounding the immobilized dye (yellow star). The interfaces between the layers influence the fluorescence lifetime of the dye.

1.3. Spectra at the temperature of liquid nitrogen

To measure spectra, a mirror is placed in the path guiding the emitted light onto a transmission grating (VPH 600 GR, Edmund Optics, Barrington, NJ). The resulting spectrum is recorded by a CCD-camera (sensicam qe, PCO AG, Kelheim, Germany). Measurements at room temperature/77K were conducted with a peptide concentration of 1 µM/5 µM, laser intensity of 1.2 kW/cm² /2.4 kW/cm² and an integration time *t* of the CCD-camera of 100 ms/1s. The laser lines of 488 nm, 594 nm, and 633 nm were used to calibrate the spectra. No filter, except of the dichroic mirror, was placed in the detection path to avoid distortion of the spectra. Comparison of the emission spectrum of AF488 measured at room temperature in a fluorometer (Perkin Elmer, LS 50 B, Waltham, MA) with that measured in the microscope revealed no significant difference (data not shown).

FIG. S3 shows the emission spectra of AF488 and AF594 bound to the peptide measured in the microscope at room temperature and at 77 K. The reflected/scattered laser light at 488 nm and 594 nm has a high intensity due to missing filters, and partly overlaps the emission spectra. As expected, the spectra shift towards shorter wavelengths upon freezing. The shift amounts to ≈ 10 nm for AF488 and ≈ 15 nm for AF594.

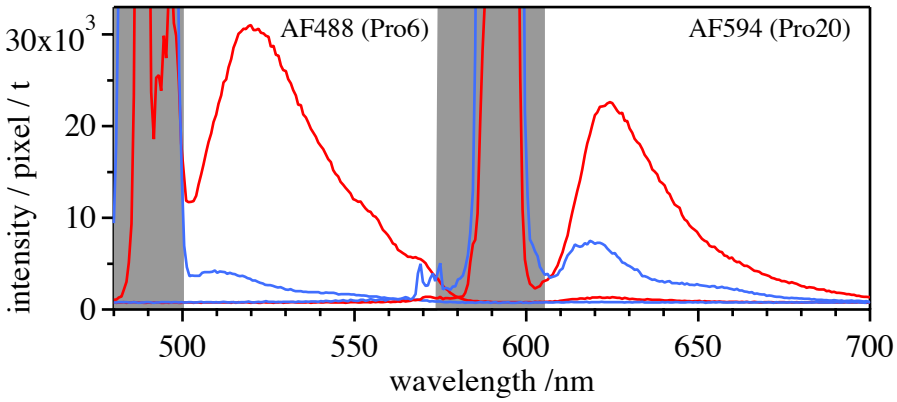

FIG. S3: Emission spectra of AF488 bound to proline 6 and AF594 bound to proline 20 at room temperature and at 77 K. The spectra at room temperature are shown in red; those at 77 K are shown in blue. The grey bar covers the reflected/scattered light of the exciting lasers, 488 nm for the donor and 594 nm for the acceptor. Due to the minimization of solvent relaxation upon freezing, the Stokes shift decreases and the emission spectra shift to smaller wavelengths.

2. Correction factor γ, background correction and crosstalk in the experiment

The transfer efficiency is determined from the fluorescence intensities of the donor, *D,* and the acceptor, *A,* the background signal in the donor channel, B_D, and in the acceptor channel, B_A, according to:

$$E = \frac{A - B_A}{A - B_A + \gamma(D - B_D)}$$

γ, the correction factor, which accounts for the detection efficiency of the donor channel η_D and the acceptor channel η_A, and for the fluorescence quantum yield of both fluorophores, Φ_D and Φ_A, is defined as $\gamma = \eta_A \Phi_A / \eta_D \Phi_D$.

The theoretical detection efficiencies of each channel were calculated with the transmission properties of the dichroic mirror (z-488-594, Chroma, Bellows Falls, VT), the objective (CFI Achromat 60 X, NA 0.8, Nikon), and the respective band-pass filter (HQ532/70 or 650/100, Chroma) as well as the detection efficiency of the APD (SPCM AQRH 14, Perkin Elmer, Waltham, MA). They amount to η_D = 0.328 and η_A = 0.245, taking into account the blue shift of the emission spectra of the donor and the acceptor (see FIG. S3 and Suppl. Section 1.3.).

The donor quantum yield Φ_D amounts to 0.93, determined with the measured fluorescence lifetime in Suppl. Section 1.3. and calculated in Suppl. Chapter 4. The acceptor quantum yield is estimated using the ratio of the radiative rates of the donor dye at room temperature and at 77 K. Near the interface the radiative rate of the donor increases by a factor of 32 %, which is supposed to be the same for the acceptor dye[5], resulting in an acceptor quantum yield of Φ_A = 0.71.

The background signal of each channel is calculated by averaging the intensity per pixel and bin time (1 ms) of image sections, which do not exhibit fluorescent molecules. It amounts to B_A = 4 photons/pixel/ms in the acceptor channel and to B_D = 2 photons/pixel/ms in the donor channel.

Crosstalk of the fluorophores, which is the detection of donor photons in the acceptor channel and vice versa, can be neglected for the dyes used here.

3. Influence of the analysis of the stoichiometry on the measured transfer efficiency distributions

The alternating laser excitation enables direct excitation of the donor and the acceptor, and thus analysis of the transfer efficiency as well as of the stoichiometry (see text Section 3.4.). For a start, the distributions of the transfer efficiencies are calculated taking the sum threshold $(A+D)_{ex488}$ for the intensity of the donor D and the acceptor A during blue (488 nm) excitation to discard background intensities. In the resulting distributions, shown in FIG. S4, both proline 6 and proline 20 show a significant amount of low transfer efficiencies between 0 and 0.2.

Low transfer efficiencies can arise from large fluorophore distances, an orientation factor close to zero or due to an inactive/missing acceptor. Polypeptides lacking an active acceptor can be sorted out by checking the acceptor's presence with an additional threshold criterion for the acceptor intensity A_{ex594} during orange (594 nm) excitation. Thus, only spots, which, additionally to the sum threshold, exceed the threshold during direct acceptor excitation, are taken into account for the final transfer efficiency histogram (FIG. S4).

The fraction of low transfer efficiencies of proline 6 has vanished completely due to the acceptor threshold while for proline 20 the fraction is reduced by about a half. Interestingly, molecules with higher transfer efficiencies are rejected as well in both histograms. Due to the selective excitation of a dye, which depends on the orientation of the dye's transition moment with respect to the polarization of the exciting light, not all fluorophores are excited equiprobable[6]. Hence, it is possible that the donor via FRET can excite the acceptor, but direct excitation by the orange (594 nm) laser light is to weak. That means, transfer efficiency of a dye pair can be detected during blue excitation, but the acceptor signal of the direct excitation is too weak to exceed the required acceptor threshold for the efficiency histogram.

The number of detected proline 6 peptides is decreased from 881 to 418 by the acceptor threshold and for proline 20 from 1008 to 541 molecules.

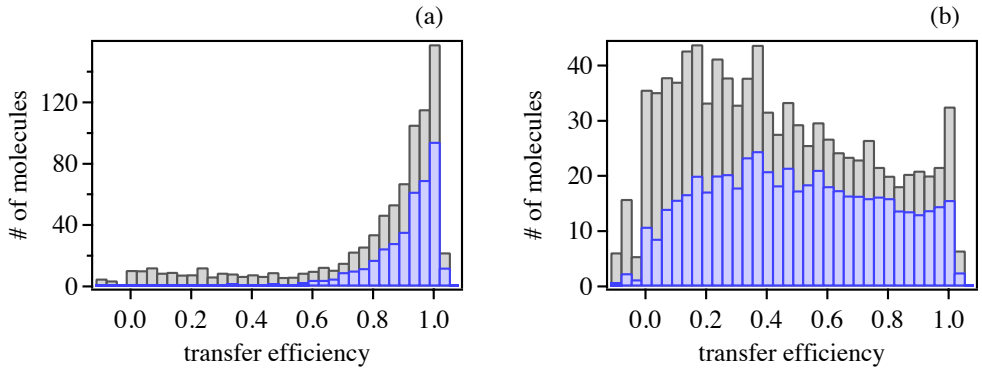

FIG. S4: Transfer efficiency distribution with and without acceptor threshold. The transfer efficiency distribution of all polypeptide pairs exceeding the sum threshold $(A+D)_{ex488}$ during the blue (488 nm) excitation is shown in grey for proline 6 (a) and proline 20 (b). Adding a threshold criterion for the acceptor intensity A_{ex594} during orange (594 nm) excitation, molecules with no or with an inactive acceptor are sorted out. The resulting histograms are shown in blue.

4. Influence of the shot noise – comparison of histograms over spots vs. over pixels

In order to evaluate the sensitivity of the histograms on the chosen method for data selection, we compared histograms over pixels (see Section 3.4.) with histograms over spots (FIG. S5) and found no significant influence.

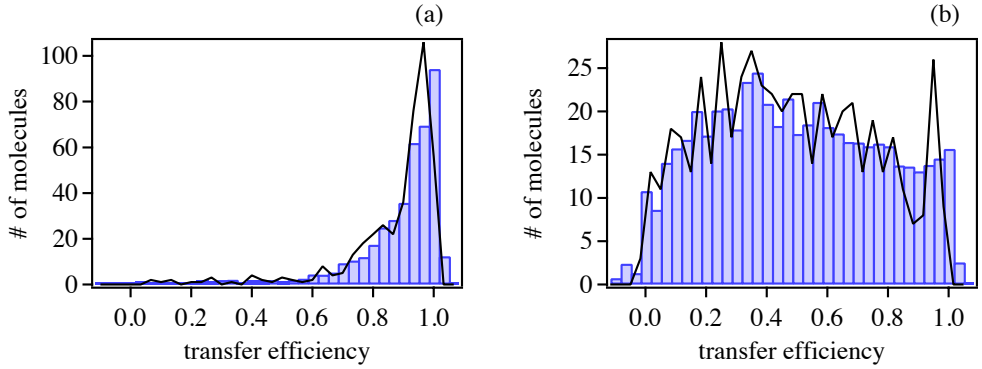

FIG. S5: Transfer efficiency histograms of proline 6 (a) and proline 20 (b) determined over pixels in blue bars (the histogram of pixels in one spot is normalized to an area of one) and with the average transfer efficiency per spot as black line.

5. Förster-radius R_0 for simulated FRET distributions

To simulate transfer efficiency distribution with Monte-Carlo methods (Section 4.2.), Förster radii needed to be calculated, according to[6]:

$$R_0 = 0.211\kappa^2 J(\lambda)\Phi_D/n^4 \qquad \text{(S1)}$$

The overlap integral $J(\lambda)$ is defined as $\int_0^\infty F_D(\lambda)\varepsilon_A(\lambda)\lambda^4 d\lambda$, with $\Phi_D(\lambda)$, the normalized emission of the donor dye; $\varepsilon_A(\lambda)$, the extinction of the acceptor dye; and λ, the wavelength. Both, the emission spectrum of the donor and the absorption spectrum of the acceptor are taken from vendor (Invitrogen, Life Technologies, Carlsbad, CA), but, the emission spectrum of the donor was shifted to shorter wavelength by 10 nm, as determined experimentally (see FIG. S3 and Suppl. Section 1.3.).

The donor quantum yield of fluorescence Φ_D was calculated based on the measured fluorescence lifetimes at ambient temperature and 77 K (see Suppl. Section 1.2.). The donor quantum yield at ambient temperature accounts to Φ_D = 0.91, calculated using $\Phi_D = \tau_0 / \tau_n$ with τ_n, the natural lifetime of the donor (τ_n = 4.5 ns, Invitrogen) and τ_0, the measured lifetime at ambient temperature (τ_0 = 4.1 ns, see FIG. S2 and Suppl. Section 1.2.). At 77 K, the fluorescence lifetime is reduced to τ_0 = 3.2 ns, indicating a higher radiative rate. Assuming that the non-radiative rate stays constant at 77 K, the quantum yield increases to 0.93. This increase of quantum yield has been observed for other fluorophores at low temperatures[2]. However, in our case, it is mainly the increase of the radiative rate due to the interface effect explained in Suppl. Section 1.2. that leads to the increase of the quantum yield of fluorescence. We'd like to stress that non-radiative rates are small compared to the radiative rate for Alexa Fluor 488, so that even changes in the non-radiative rates would only slightly change the donor quantum yield.

The refractive index n of ice, taken for the calculation of R_0, is 1.31 at 77 K.

The orientation factor κ^2 takes into account the mutual orientation of the dyes, which have a static random orientation in a frozen matrix. In the simulation for every molecule a random orientation was generated by Monte-Carlo methods (see Section 4.2.).

Fig. S6 shows the distribution of Förster radii obtained by equation (S1), which is peaked around 6 nm with a width dominated by the distribution of orientation factors.

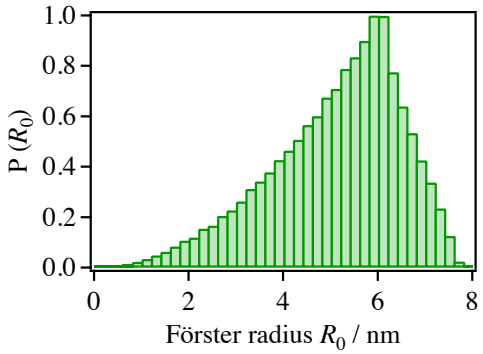

FIG. S6: Distribution of the Förster radii for an ensemble of static, randomly oriented donor-acceptor pairs under the experimental conditions of this work.

6. Simulated end-to-end distances including *cis-trans*-isomerism and dye distances

The other input for the simulation of the FRET efficiencies is the distance between the dyes. This distance was simulated as described in the main text (see Section 4.2.). Fig. S7 shows the resulting distributions for prolines with no, one, two, and three *cis*-bonds, respectively, together with the resulting overall distribution including flexibility of the dye linkers. They are peaked at 2 nm for proline 6 and 6.5 nm for proline 20, respectively.

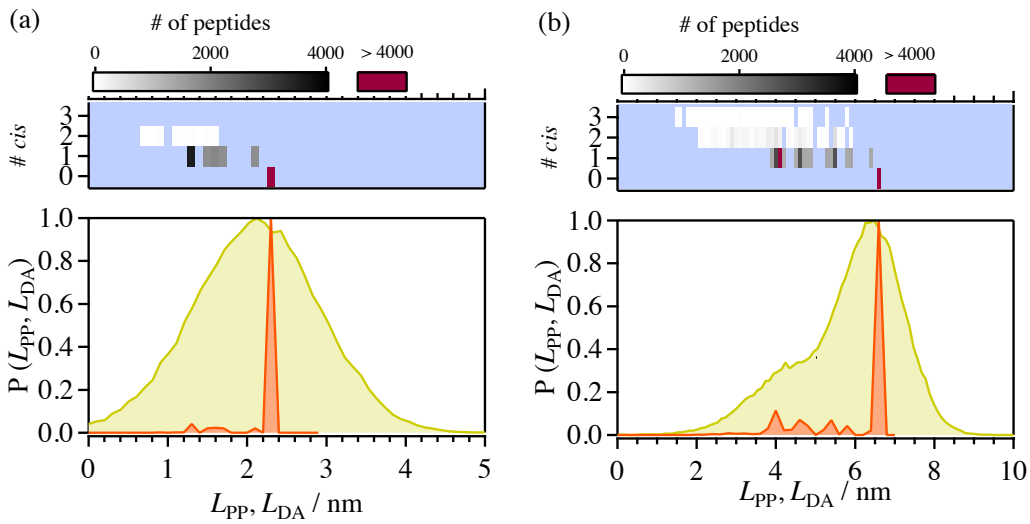

FIG. S7: Theoretical end-to-end distances L_{PP} and dye distances L_{DA}:

Bottom: The probability distributions of end-to-end-distances L_{PP} (orange) of proline 6 (a) and proline 20 (b) were simulated by Monte-Carlo methods using the known dihedral angles of a polyproline II helix (see text Section 4.2.). The end-to-end-distances vary due to the included fraction of 2 % *cis*-bonds, which lead to kinks in the chain on different positions[7]. The major part of both peptides does not contain any *cis*-bond leading to the largest end-to-end-distance, *i.e.* 2.3 nm for proline 6 and 6.6 nm for proline 20.

The probabilities of the dye distances L_{DA} (green) are calculated from the simulated end-to-end-distances L_{PP} and an additional distribution of the linker lengths of the dyes. A Gaussian distance distribution with a mean of -0.2 nm and a standard deviation of 0.76 nm, taken from the result of a molecular dynamics simulation in Ref. [8], accounts for the flexibility of the dye linkers.

Top: Mapping of the number of *cis*-bonds in a peptide chain relating to the end-to-end-distance of 10^5 simulated peptides (proline 6 (a), proline 20 (b)). Blank fields are shown in blue. Amounts of more than 4000 peptides are shown in red. Only 11 % of the proline 6 peptides contain one or, very rarely, two *cis*-bonds, which can shorten the distance by about

1 nm [7]. The amount of kinked peptides is larger for proline 20 (33 %). A kink in the middle of proline 20, for instance, shortens the end-to-end-distance to 4 nm [9].

7. Simulated images and E-S histograms of proline 6 and of proline 20

For the simulation of images (FIG. S8) according to the experimental conditions and based on the model of randomly oriented fluorophores, random polar angles were generated by transforming a uniform distribution into a sinusoidal distribution via the arcsine function. Random azimuthal angles were generated according to a uniform distribution. Both, donor and acceptor dipole orientations were simulated independently. The polar angle dependent absorption was derived on the basis of the components of the electrical field in the focus of the microscope objective[10-13].

Then, for every molecule the photon emission rates for the FRET donor and acceptor were calculated based on the beforehand simulated transfer efficiency (section 4.2. in the main paper) and scaled according to the orientation dependent excitation and detection probabilities. The emission rates were fed into 2D Gaussians with random positions and a width corresponding to the resolution of the microscope from the experiment. The positions were generated in such a way that the areal density in the simulation matches the experiment. Finally, the photon emission rates were subjected to a Poisson distribution to account for shot noise.

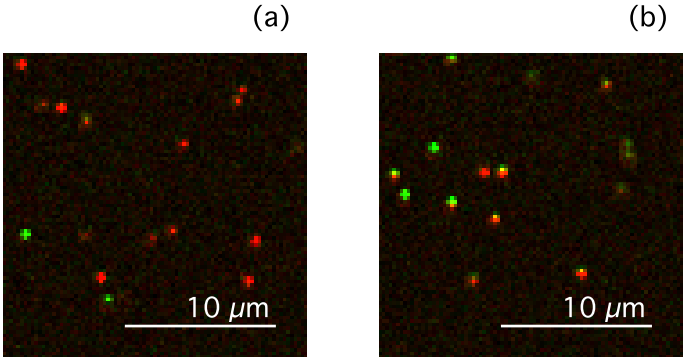

FIG. S8: Simulated intensities of the donor (green) and the acceptor (red) for proline 6 (a) and proline 20 (b) according to simulated transfer efficiencies are shown. Intensities in both channels appear yellowish. Different colors within one spot result from photon shot noise. Shot noise, an excitation rate depending on the absorption-dipole of the dyes and a detection efficiency depending on the emission-dipole of the dyes were included to account for all aspects of the experiment. Shown are sections of larger images of 10^5 molecules. The areal density corresponds to that in the experiment. The molecules are randomly placed.

In order to evaluate the experimental data, the analysis of simulated images is shown in FIG. S9. In the simulations, the orientation-dependent excitation as well as detection efficiency was taken into account. The simulation showed best agreement with the experiment when a fraction of 20 % of molecules bearing only a donor dye was included in the simulation. Maximal fluorescence intensities of the dyes and threshold criteria were chosen according to the experiment. Roughly 20 % of the simulated molecules had intensities below the thresholds due to an unfavorable orientation of the absorption dipole of the donor or acceptor with respect to the incoming laser light, which was elliptically polarized after the beam splitter. Although the *E*-*S* histograms of the simulated data are similar to the histograms of the experimental data, there are still slight differences. In particular, in the experiment, there is a larger population of spots with $S \approx 1$ and transfer efficiency values distributed between 0 and 1. The origin of this small population, which could be impurities in the sample, needs to be further investigated.

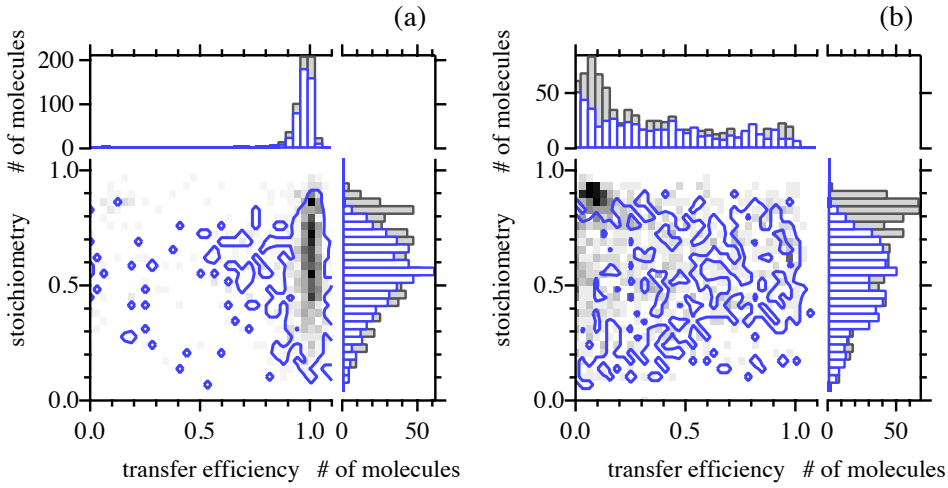

FIG. S9: Simulated *E*-*S* histograms of proline 6 (a) and of proline 20 (b) for a number of molecules similar to the experiment (≈ 1000). The grey scaled images show unfiltered data, *i.e.* all data exceeding the sum threshold but not the threshold for direct acceptor excitation. The blue contour plots show the filtered data, *i.e.* only molecules bearing donor and acceptor. The one-dimensional histograms of *E* and *S* are plotted aside, unfiltered in grey and filtered in blue.

8. Transfer efficiency distributions of proline 6 and of proline 20 at room temperature

Transfer efficiency histograms measured at room temperature in solution for proline 6 and for proline 20 are shown in FIG. S10. Experiments were conducted on the same confocal microscope as described in Section 3.1. using a water immersion objective (CFI Plan Apochromat 60x WI, Nikon) and a standard sample holder supporting the cover slip. The excitation intensity of the 488 nm laser line was 12 kW/cm². Samples were diluted in 50 mM sodium phosphate buffer, pH 7.0, containing 0.001 % (v/v) Tween 20 (Carl Roth), to a

concentration of 100 pM. Transfer efficiencies were calculated using equation $E=A/(A+\gamma D)$ (see Suppl. Chapter 2), using a sum threshold ($A+D$) of 70 counts per millisecond and γ of 0.83. For comparison, simple MC simulations were conducted. To this end, molecules, diffusing through the confocal volume, emit photons according to the molecular brightness of the dyes in the experiment. The simulated intensities were subjected Poisson noise so that the simulated curves show a shot noise limited distribution of the transfer efficiencies.

The transfer efficiencies of proline 6 in solution are close to unity and show, compared to the simulation, a shot noise limited distribution. Proline 20 shows a broad distribution of transfer efficiencies with an average of about 0.41. The histogram of the shot noise limited simulation for proline 20 shows clearly the broadening of the histogram due to the conformational heterogeneity of proline 20 (see Chapter 4.2.), which is discussed in detail in the literature[7, 8].

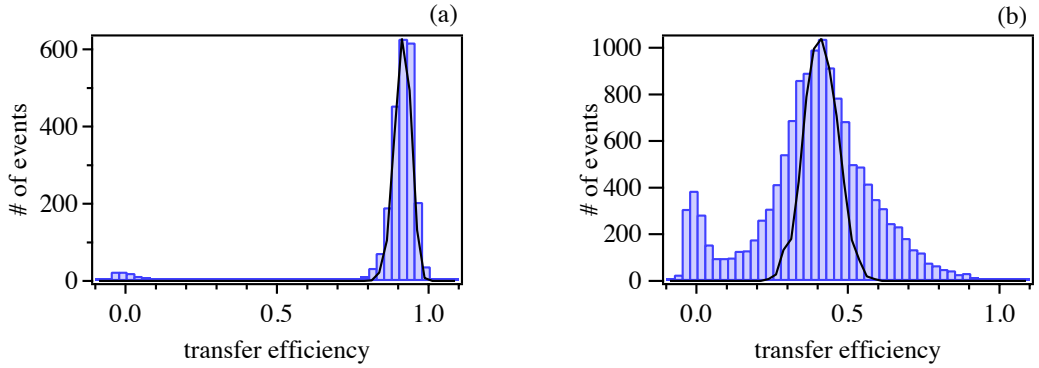

FIG. S10: Distributions of the transfer efficiencies of proline 6 (a) and proline 20 (b) measured at room temperature are illustrated as bars. A shot noise limited distribution, simulated with the average intensities from the experiment, is shown as black curve. The peaks close to zero are due to donor only molecules.

References

1. T. Ha, T. A. Laurence, D. S. Chemla and S. Weiss, *J. Phys. Chem. B*, 1999, **103**, 6839-6850.
2. L. C. T. Shoute, V. J. MacKenzie, K. J. Falk, H. K. Sinha, A. Warsylewicz and R. P. Steer, *Phys. Chem. Chem. Phys.*, 2000, **2**, 1-9.
3. C. Tietz, O. Chekhlov, A. Drabenstedt, J. Schuster and J. Wrachtrup, *J. Phys. Chem. B*, 1999, **103**, 6328-6333.
4. C. T. Lin, A. M. Mahloudji, L. Li and M. W. Hsiao, *Chem. Phys. Lett.*, 1992, **193**, 8-16.
5. M. Kreiter, M. Prummer, B. Hecht and U. P. Wild, *J. Chem. Phys.*, 2002, **117**, 9430-9433.
6. J. R. Lakowicz, *Principles of Fluorescence Spectroscopy*, 3 edn., Springer, 2006.
7. R. B. Best, K. A. Merchant, I. V. Gopich, B. Schuler, A. Bax and W. A. Eaton, *Proc. Natl. Acad. Sci. U. S. A.*, 2007, **104**, 18964-18969.
8. M. Hoefling, N. Lima, D. Haenni, C. A. M. Seidel, B. Schuler and H. Grubmüller, *Plos One*, 2011, **6**.
9. S. Doose, H. Neuweiler, H. Barsch and M. Sauer, *Proc. Natl. Acad. Sci. U. S. A.*, 2007, **104**, 17400-17405.
10. M. A. Lieb, J. M. Zavislan and L. Novotny, *J. Opt. Soc. Am. B*, 2004, **21**, 1210-1215.
11. J. T. Fourkas, *Opt. Lett.*, 2001, **26**, 211-213.
12. R. Börner, D. Kowerko, S. Krause, C. von Borczyskowski and C. G. Hübner, *J. Chem. Phys.*, 2012, **137**.
13. J. Hohlbein and C. G. Hübner, *J. Chem. Phys.*, 2008, **129**.